Acta Materialia 321 (2026) 122807

Contents lists available at ScienceDirect

Acta Materialia

journal homepage: www.elsevier.com/locate/actamat

Full length article

Predicting glass-forming ability in binary alloys by machine learning

Yifei He [a,b,†], Guannan Liu [a,b,†], Salena Huang [a,b], Sebastian Kube [c], Sungwoo Sohn [a], Xiaorui Xiong [i], Mark D. Shattuck [d], Corey S. O'Hern [a,b,e,f], Anna Gilbert [g,h], Jan Schroers [a,b,j,*]

[a] Department of Materials Science, Yale University, New Haven, Connecticut, 06520, USA
[b] Department of Mechanical Engineering, Yale University, New Haven, Connecticut, 06520, USA
[c] Department of Materials Science and Engineering, University of Wisconsin – Madison, Madison, Wisconsin, 53706, USA
[d] Benjamin Levich Institute and Physics Department, The City College of the City University of New York, New York, New York, 10031, USA
[e] Department of Applied Physics, Yale University, New Haven, Connecticut, 06520, USA
[f] Department of Physics, Yale University, New Haven, Connecticut, 06520, USA
[g] Department of Electrical & Computer Engineering, Yale University, New Haven, Connecticut, 06520, USA
[h] Department of Statistics & Data Science, Yale University, New Haven, Connecticut, 06520, USA
[i] Department of Computer Science, Yale University, New Haven, Connecticut, 06520, USA
[j] Institute of Materials Research, Tohoku University, Sendai, Japan

ARTICLE INFO

Keywords:
Machine learning
metallic glass
glass-forming ability
critical cooling rate
BMG
sputtering
combinatorial materials science

ABSTRACT

Predicting metallic glass-forming ability (GFA) through machine learning has been challenging. Among the reasons for the challenge are limited, biased and inconsistent experimental data, binary vs continuous labeling, and limited feature representation particularly for multicomponent alloys. To address these challenges, we restrict the problem to binary alloys and base the training data on experiments spanning a representative fraction of ~ 20% of binary alloys, which have been synthesized through sputtering and its atomic structure characterized.

Consistent in quality and sufficient quantity of binary sputtering data with continuously labeled GFA quantified in the critical cooling rates (R_c) are constructed, and Physically Informed features based on atomic size, crystal mismatch, Miedema-based mixing enthalpy, and melting temperature are employed to describe the alloy in terms of its R_c. Using the Physically Informed features, the random forest model predicts the critical cooling rate with a mean absolute percentage error of ~18% (MAPE in $\log_{10}$ (R_c) space), compared to a simple benchmark model reaching a MAPE of 28%. However, attempts to use this binary model to predict R_c in ternary alloys are ineffective; using the ML model trained on binary data to predict R_c in ternary alloys results in a MAPE of ~36% for sputtered ternary alloys and ~ 89% for ternary BMG formers. Such poor performance suggests that the mixing complexity in ternary alloys is not captured in binary alloys.

Overall, we argue that while addressing previous challenges in predicting GFA through ML, the models achieve statistically improved predictive performance while retaining a physically interpretable feature set. However, the achieved predictions remain coarse, indicating additional limitations (e.g., label uncertainty, missing higher-order mixing descriptors, process dependence, etc.) that constrain precise Rc prediction. Most fundamentally, the discreteness of atoms remains the limiting factor from using ML strategies to precisely predict glass-forming ability of alloys.

1. Introduction

Machine learning (ML) has been widely used in an attempt to predict novel complex materials such as metallic glass formers [1–7], high-entropy alloys [8–10], superalloys [11,12], or phenomena such as the Hall-Petch relationship [13], and aspects of phase diagrams [14,15]. Despite the "high accuracy" often achieved in cross-validation, an actual prediction of novel metallic glass compositions that are significantly

* Corresponding author.
E-mail address: jan.schroers@yale.edu (J. Schroers).
† These authors contributed equally to this work.

https://doi.org/10.1016/j.actamat.2026.122807
Received 10 July 2026; Received in revised form 10 September 2026; Accepted 20 September 2026
Available online 23 September 2026
1359-6454/© 2026 Acta Materialia Inc. Published by Elsevier Inc. All rights are reserved, including those for text and data mining, AI training, and similar technologies.

different from the training data and exhibit high glass-forming ability has not been achieved. Previous analysis have identified several origins for the shortcomings that hinder ML algorithms from predicting metallic glasses [16] including:

- *Binary vs. Continuous Labeling*: ML models in materials science attempt to describe complex phenomena by employing binary labeling systems [1,3,17–19] (representative examples include: (i) stability classification (stable vs. unstable) based on formation energy; (ii) superconductivity classification (superconducting vs. non-superconducting) based on the critical temperature; and (iii) glass-forming ability classification (glass-forming vs. non-glass-forming) based on experimental observations such as the critical cooling rate, etc.). This approach, while computationally convenient, oversimplifies the problem and leads to a significant loss of critical information. Continuous labeling systems are required to represent the complexity of the materials science problem. For example, for bulk metallic glass formation [1,3,17], binary labels of glass or no glass formation have been used; however, the critical cooling rate which quantifies the glass-forming ability, varies continuously among alloys by ~14 orders of magnitude [20,21].
- *Data Representation Bias*: Effective ML strategies rely on data that are representative in defining the imbalance problem [22]. However, materials datasets that are used often fail to accurately represent the actual probability distributions of sample labels. For instance, in the context of bulk metallic glass (BMG) formers, the actual probability of encountering a BMG former among multicomponent alloys has been estimated to be 1 in 10^6 [23]. However, this ratio is disproportionally represented in common alloy datasets in previous studies [1,3,17], where the likelihood can be as high as ~ 1 in 2 [18,23]. Such an imbalance problem makes models inefficient, particularly if feature representation of the problem (glass-forming ability) is limited [17,24,25]. It is important to mention that ML models when class imbalance is extreme, as in the BMG case (1 in 10^6), tend to short-circuit and only predict no-glass formers [26–28]. However, a more balanced compromise between the extreme uneven class representation and random sampling is required to make models efficient [24,25].
- *Feature Representation and Bridging Elemental Properties to Alloy Features*: A general challenge in applying ML to materials science problems is representing a material through quantifiable features that map to a label (here glass-forming ability). For alloys, the mixing behavior of the constituent elements is key to many wide-ranging phenomena and properties, including glass-forming ability [29], single-phase solid solutions (high-entropy alloys) [30,31], stable nanocrystalline alloys [32–34], superconducting critical temperature [19], topological behavior [35] and liquidus temperature [14]. Typically, physics-based models have been developed to describe such mixing behavior [36] which, due to their assumptions, are approximating the real behavior and are often limited to the material class or problem of interest.
- *Subgrouping, Specificity and Accuracy of General Models*:

  Taking the example of metallic glass formation, it has been suggested by Inoue that motifs for glass formation vary for various subgroups of alloys [37], which was later confirmed through ML and data science strategies [38]. Recently, it has also been suggested that glass formation motifs change with the applied cooling rate [21]. As these findings show that metallic glass formation is not a phenomenon that can be generally described for all alloys and cooling conditions, but instead is more specific, it is reasonable to assume that the same is true when attempting to describe glass formation through ML algorithms. In fact, when subgrouping alloys through physical insights more accurate models have been achieved [38].

To address these shortcomings, we synthesize and consider a dataset of sputtered binary alloys (to reduce the group of alloys considered) and quantify their glass-forming ability (GFA) through R_c using ML. This allows us to focus on binary alloys as a subgroup of metallic glass-forming alloys), use more representative data, and use R_c as a continuous label to describe the glass-forming ability.

Metallic glass (MG) formation is of significant scientific and technological interest [28,29,39,40]. From a technological standpoint, this interest is driven by the exceptional characteristics of metallic glasses; they can exhibit ceramic-like strength [41,42], metal-like superb fracture toughness and bending ductility [43–47] combined with other properties [45,47–50], as well as plastic-like processability [51–55]. For scientific inquiry, MGs provide a convenient spatial and temporal window to explore the structure of glasses and liquids [56–58] and their structure-property relationships [59–61], and the critical cooling rates measure the stability of competing crystalline phases relative to the glass. However, due to the complex nature of MG formation, accurately predicting the GFA of alloys remains a challenging endeavor and experimental data are limited and inconsistent due to the highly elaborate measurement requirements.

In this study, we utilize binary alloy libraries on glass formation which have been acquired using fast combinatorial fabrication paired with high-throughput characterization strategies [31,62]. After experimentally generating these data, they are carefully curated to mitigate the aforementioned issues through several key improvements: 1) A significant and randomly selected fraction of all practical binary alloys is determined and used in this data set. Thereby, the data better represent the problem of glass formation; 2) continuous labeling of GFA through quantifiable R_c; 3) a more accurate representation of alloy mixing through alloy features, enabled by simpler mixing of binary alloys compared to the mixing in higher-order systems.

Physically Informed (PI) features $\in \mathbb{R}^7$(Section 2.3) are constructed to represent each alloy using properties of its constituents and its mixing behavior. We then build a ML model using random forest regression and neural networks to predict the critical cooling rate of alloys and perform leave-one-system-out tests on each binary alloy system. The resulting mean absolute percentage error (MAPE) of predicting the critical cooling rate of binary systems is ~18%. This error corresponds to 1.9 orders of magnitude in the critical cooling rate spectrum (for more details, see **Supplementary 1.1**). In comparison, a simple baseline model used as a benchmark yields a significantly higher MAPE of ~28%, which underscores the advantage of our integrated framework that combines advanced machine learning algorithms, physically informed descriptors, and a continuous reformulation of the glass-forming prediction problem.

To better understand glass formation in binary alloys, we examine the model-derived feature importance in binary alloys. We find that atomic size difference, crystal mismatch, and Miedema-based mixing enthalpy emerge as the most influential descriptors in our model. Additionally, we explore whether one can use the ML models trained on binary alloys to make predictions for ternary alloys. We find that even though some specific systems can be predicted reasonably well, generally this transfer strategy performs poorly on average when models trained on lower-order systems are applied to higher-order systems. The MAPE of predicting sputtering ternary glass formers is ~36%, and the MAPE of predicting ternary BMGs is ~89%.

2. Methods

2.1. Sample Fabrication and Characterization

Binary alloys have been fabricated through combinatorial co-sputtering (Figure 1 a) [21,62]. This process involved the synthesis of 57 compositional libraries (alloy systems), using two confocal sputtering targets. Each alloy system, which is represented in one library, is represented by 66 distinct alloys. Their composition varies from approximately $A_{95}B_5$ to A_5B_{95}, resulting in a total of ~3,800 unique alloys. The chemical composition of the alloys is characterized using energy-dispersive X-ray (EDX) analysis (Figure 1 b). High throughput sy

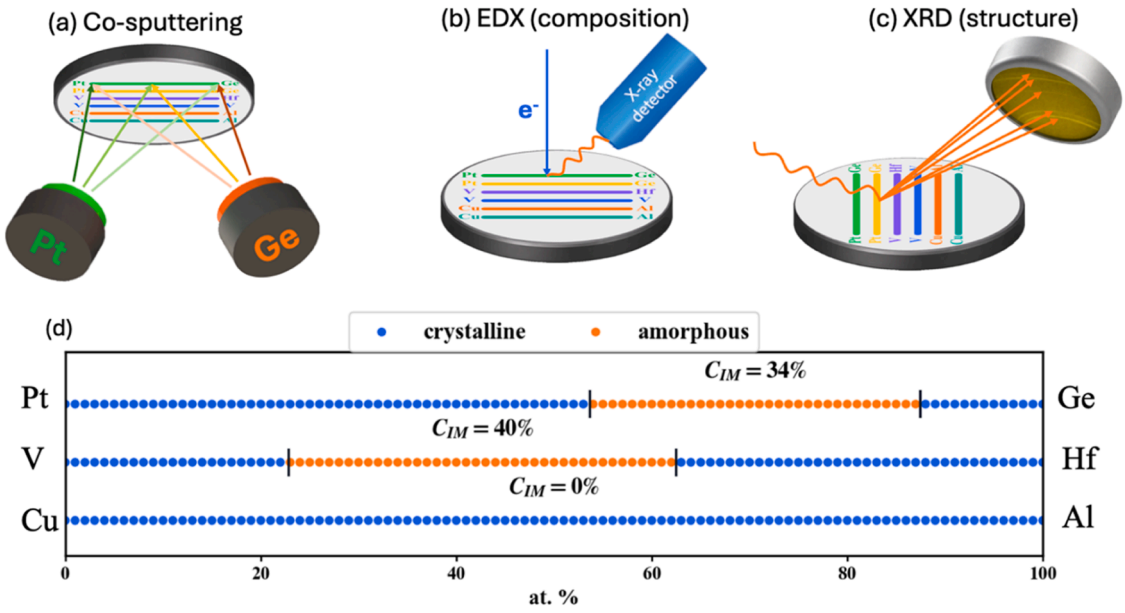


Figure 1. Combinatorial fabrication and high-throughput characterization of binary alloy libraries. a) Using magnetron co-sputtering, 66 distinct compositions (alloys) are fabricated for each binary alloy system. b) Energy-dispersive X-ray (EDX) is employed to determine the chemical composition of the alloys. c) Synchrotron X-ray Diffraction (XRD) mapping is utilized to determine the structure of the alloys, distinguishing between amorphous and crystalline forms. (d) The range in composition of amorphous vs. crystalline structures for three example alloy systems.

nchrotron X-ray diffraction (XRD) mapping (Figure 1 c) is used to determine the structure of the alloys, specifically identifying whether they exhibit an amorphous or crystalline atomic structure. Experimental details on the fabrication and characterization [21] are given in Sections 2.1.1 and 2.1.2.

2.1.1. *Combinatorial Co-sputtering Fabrication*

The binary alloy libraries were fabricated through confocal DC Magnetron co-sputtering (AJA International ATC2200), illustrated in Figure 1 a. Sputtering targets with a purity of at least 99.95% (AJA International and Kurt J. Lesker Company) were employed. For substrates, we use 4-inch diameter wafers (UniversityWafer Inc.), with sapphire wafers for Si-containing binaries and silicon wafers with a 1 μm thermal oxide layer for all other binaries. Deposition is restricted to specific rows (3 mm height and 83 mm length) using steel masks (0.01" thickness) that can be exchanged without opening the chamber. The combinatorial deposition process for each AB binary system, for which the element targets are arranged at an angle relative to the substrate, creates a compositional gradient within a row, ranging from approximately A_5B_{95} to $A_{50}B_{50}$ in the first and $A_{50}B_{50}$ to $A_{95}B_5$ in the second row. These compositions are controlled by adjusting the deposition rates through the applied power. Prior to deposition, the chamber is evacuated to 5.0 $\times$ 10^{-7} Torr and the films were sputtered in ultra-high purity argon gas at a pressure of 5.8 $\times$ 10^{-3} Torr.

2.1.2. *High-throughput Characterization*

The compositional gradient rows were characterized using EDX and XRD techniques. EDX analysis was performed with a Helios G4 Focused Ion Beam – Scanning Electron Microscope (UltraDry EDX detector, 25 kV accelerating voltage). For XRD, the Stanford Synchrotron Radiation Lightsource (SSRL) at SLAC National Accelerator Laboratory (beamline 1-5, 12.7 keV photon energy) was utilized. Automated routines control the positioning of the samples (xy-coordinates), allowing for measurements every 2.5 mm along the row length, ensuring a thorough and detailed characterization of the compositional variations.

2.2. *Continuous Labeling of GFA using Critical Cooling Rate R_c*

The GFA of binary alloys is characterized as either amorphous or crystalline based on XRD measurements. To advance beyond this binary labeling, we use the critical cooling rate (R_c) as a continuous measure of GFA. R_c is the minimum cooling rate necessary to prevent crystallization during solidification, thereby enabling the formation of a glass with an amorphous atomic structure [56,60,63]. R_c can vary within metallic elements and alloys by ~14 orders of magnitude [62,64]. Thus, R_c contains more information than a binary labeling (glass/crystal formation at a given cooling rate).

Experimentally determining R_c for alloys presents a significant challenge and, as a consequence, has been carried out for only very few alloys [1,20,65–67]. Due to the challenges associated with direct measurements of the critical cooling rate, we propose a fitting method to estimate R_c from experimental data. Specifically, we consider four data points per alloy system (the starting and ending points of the two pure elements in each binary alloy and two boundary points between crystalline and amorphous regions). We assume the critical cooling rate for pure metals to be ~10^{14} K/s [68,69]. This yields two data points at pure A and B for the A-B alloy system (see Figure 2 green dots). Assuming that magnetron sputtering of metals results in a "cooling rate" of 10^8 K/s [62], we can identify the two alloys at which, as a function of composition, the solidification product changes between crystalline and amorphous (see Figure 2 red dashed lines) and $R_c = 10^8$ K/s. These four data points form the basis of our fitting approach. For the binary systems where bulk glass formers have already been reported such as NiMg, CuZr, CoMg, TaMn, GeMg, and HfFe [23,28,29], we introduce an additional data point at 10^3 K/s at the bulk-glass-forming composition.

Utilizing a quadratic spline fit, we then construct an R_c (x) curve (x is the composition) for each alloy system, for each considered binary alloy system. The resulting curve provides estimated values of R_c for each alloy. A graphical representation of the curves (Figure 2 a) highlights the continuous nature of the GFA approximation. For binary systems with no amorphous range (Figure 2 b), the two transition data points at R_c = 10^8 K/s are not available. For those alloy systems, a data point in the middle of the alloy system at $A_{50}B_{50}$ where we assume $R_c = 10^{11}$ K/s. The reasoning for such an assumption is that we consider the average

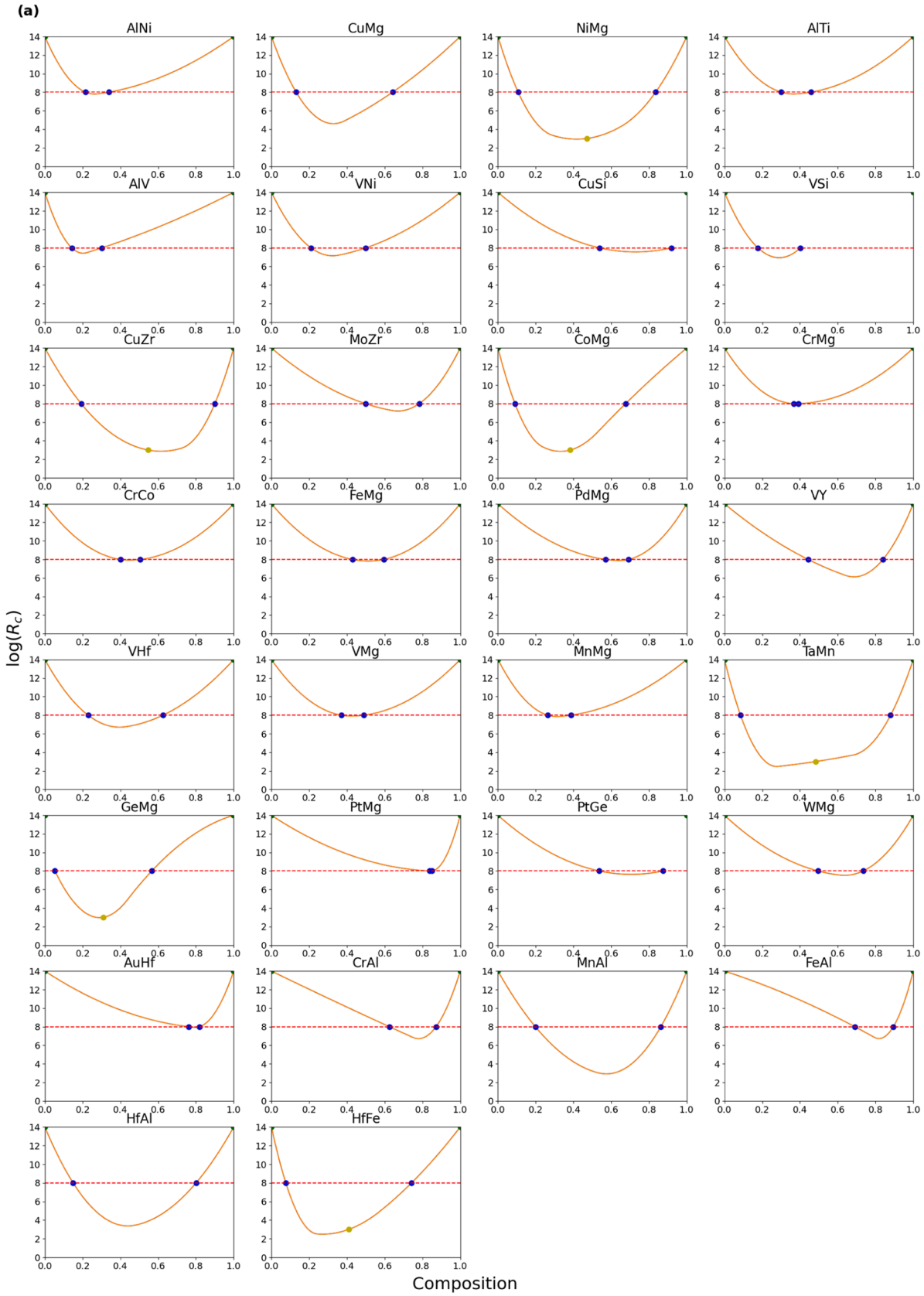


Figure 2. Quadratic spline fits to estimate the critical cooling rate (R_c) as a function of alloy composition for various binary systems. Each curve represents a distinct binary system and presents an estimation of R_c across the composition spectrum. Green dots mark experimental data for bulk glass formation. For the pure elements, $R_c = 10^{14}$ K/s is assumed. (a) The systems that form glasses at some compositions: The blue dots mark the compositional boundaries. At the dots, $R_c = 10^8$ K/s. (b) The systems for which no glass formation at any composition has been observed. The yellow dots represent the middle point of the binary system where the average atomic size difference suggests $R_c = 10^{11}$ K/s.

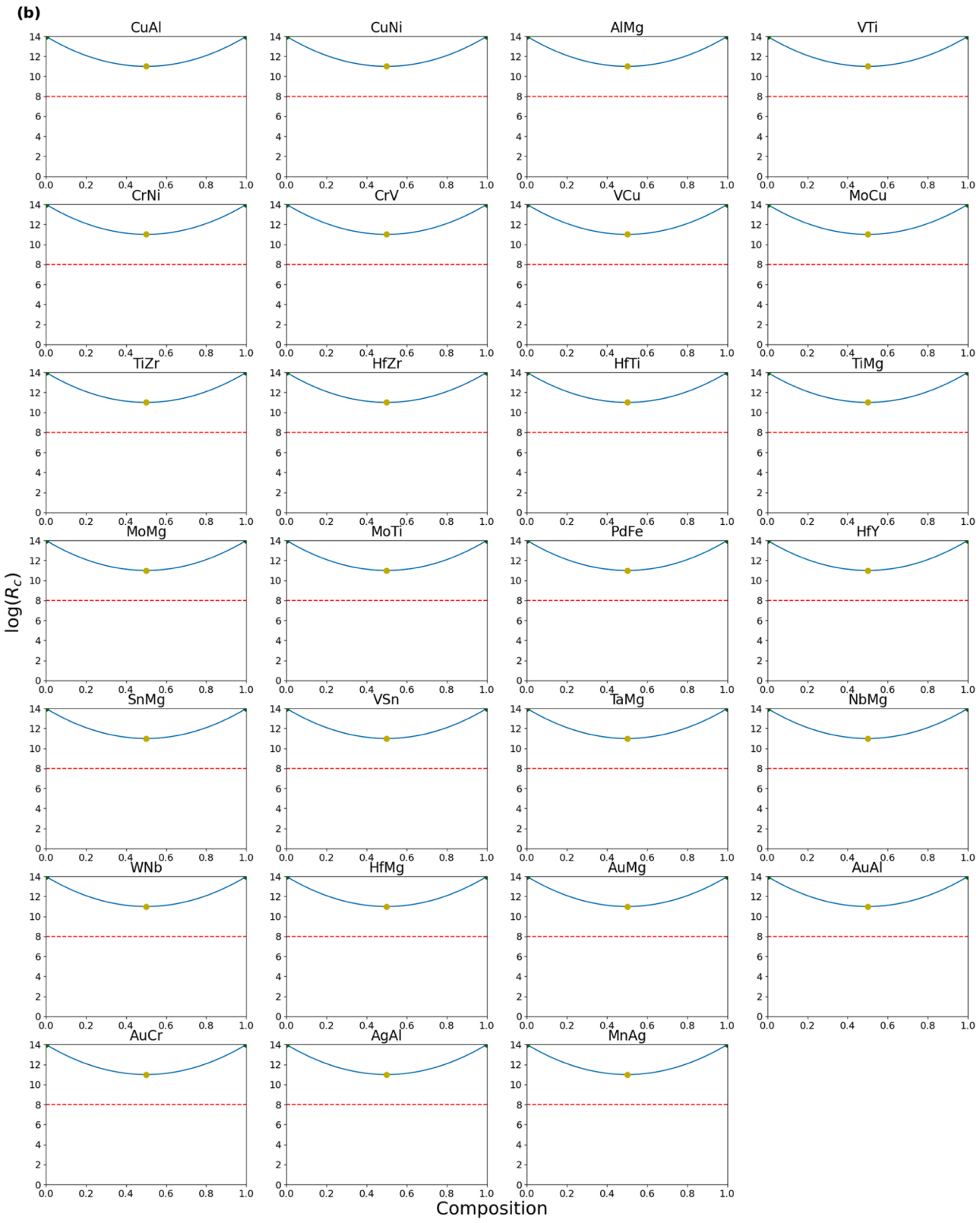


Figure 2. (*continued*).

atomic size difference in the alloys and consider the effect of the atomic size difference on the GFA [37,70].

It is important to mention that the constructed R_c (x) curves should be regarded as rough estimates rather than exact experimental ground truth. For example, the specific competing crystalline phases are not explicitly considered [71], particularly the presence of thermally stable intermetallic phases [29]. Such contributions may lead to multiple local minima in R_c within one alloy system [72], which cannot be captured by a simple quadratic-spline representation.

To evaluate the uncertainty associated with the assumed reference

cooling rates, we performed a sensitivity analysis by systematically varying the assumed sputtered boundary, pure element, and intermediate composition R_c values. As summarized in the **Supplementary 1.3**, the absolute R_c prediction error varies appreciably with these assumptions, confirming that the numerical R_c values should not be interpreted as uncertainty-free quantities. In contrast, the predicted amorphous composition boundaries are substantially less sensitive to the assumed reference values, and the dominant feature importance trends remain largely unchanged. In particular, atomic size difference and Miedema-based mixing enthalpy consistently remain among the most important descriptors, while the Crystal Mismatch 0 and Crystal Mismatch 1 features are also ranked highly in most cases.

Therefore, although the absolute magnitude of R_c is subject to uncertainty arising from the assumption to construct the R_c (x) curve, we argue that the general composition dependent trends in glass formation suggested by theoretical models [37,73] and experimental observations [37,74,75] are reasonably captured by these R_c (x) curves. Accordingly, the present framework is intended primarily for identifying relative trends and physically meaningful descriptors of glass formation behavior rather than for providing exact absolute critical cooling rates.

2.3. Feature Construction

Features are required in ML to translate raw data (here alloy compositions) into quantifiable, representative, and meaningful inputs for the development of algorithms predicting the desired output (here R_c). Effective feature construction requires an understanding of the physical mechanisms that control an alloy's critical cooling rate [29,36,37]. Specifically, we construct Physically Informed features, which are:

1. Atomic size difference, δ:

$$\delta = \sqrt{x_A \cdot \left(1 - \frac{r_A}{r_{avg}}\right)^2 + x_B \cdot \left(1 - \frac{r_B}{r_{avg}}\right)^2} \quad (1)$$

where r_A and r_B are the atomic radii of the constituent elements, and x_A and x_B are the atomic molar fractions of the elements and $r_{avg} = x_A\, r_A + x_B\, r_B$

2. Atomic size ratio Φ:

$$\Phi = \frac{r_{\max}}{r_{\min}} \quad (2)$$

where $r_{\max}$ represents the largest and $r_{\min}$ the smallest atomic radius among the constituent elements.

3. Atomic size range Δr:

$$\Delta r = r_{\max} - r_{\min} \quad (3)$$

where $r_{\max}$ represents the largest and $r_{\min}$ the smallest atomic radius among the constituent elements.

4. Crystal Mismatch 0, CSM0:

$$CSM0 = x_A \cdot x_B \cdot S_0 \quad (4)$$

where for a binary alloy A_xB_{1-x}, $S_0 = 0$ if the crystal structure of element A is the same as the crystal structure of B (for example, both BCC); $S_0 = 1$ if their crystal structures are different (for example, one is BCC, and the other one is FCC).

5. Crystal Mismatch 1, CSM1:

$$CSM1 = S_1 x_A x_B + R_p \quad (5)$$

The motivation for CSM1 is to include in the crystal structure mismatch variable the effects of the critical cooling rate [21]. To match the scale of variation of the effect of CSM1 with critical cooling rate variations, we assume the critical cooling rate for pure metals to be on the order of 10^{14} K/s [68,69] which R_p is equal to 14, and use this value as a reference scale for calibrating the relationship between CSM1 and log (R_c). For a binary alloy A_xB_{1-x}, $S_1 = -16$ if the crystal structure of element A is the same as the crystal structure of B; $S_1 = -32$ if their crystal structures are different. The coefficient S_1 is empirically calibrated such that the resulting CSM1 values align with the logarithmic scale of the critical cooling rate R_c. At x_A and x_B are both equal to 0.5, systems with identical crystal structures (S_1 = -16) yield CSM1 $\approx$ 10, corresponding to $R_c \sim 10^{10}$ K/s, whereas systems with different crystal structures (S_1 = -32) yield CSM1 $\approx$ 6, corresponding to $R_c \sim 10^6$ K/s. This design enables CSM1 to serve as a physically interpretable proxy for R_c across different alloy systems.

6. Miedema-based mixing enthalpy, ΔH:

$$\Delta H = 2 x_A x_B \varepsilon_{AB} \quad (6)$$

Here, ε_{AB} is calculated by using Miedema model [37] for the binary alloys (mixing enthalpy of equally mixed binary alloy ($A_{50}B_{50}$)) in kJ/mol.

7. Average melting temperature, T_{avg}:

$$T_{avg} = T_A \cdot x_A + T_B \cdot x_B \quad (7)$$

T_A and T_B are the melting temperatures of the elements.

For comparison, we also consider the Elemental Properties (EP) feature vector, EP$\in \mathbb{R}^{66}$ (see supplementary 1.2.1), which does not consider any mixing behavior of an alloy but instead uses known and potentially relevant properties of the alloys' constituent elements A and B. To make these features specific to an alloy, the composition of the alloy is added as two components of the 66-component EP feature vector. To benchmark these constructed features, we create benchmark features. One is the Composition feature vector $\in \mathbb{R}^{24}$ (all considered binary alloys have been made from 24 elements) which do not contain any information in the feature except its chemical composition features (see supplementary 1.2.2). Even more dramatically, we also construct Random feature vectors $\in \mathbb{R}^7$ which do not contain any information (see supplementary 1.2.3). They are constructed through 7 random and normalized numbers.

3. Results

3.1. ML Performance in Leave-One-System-Out Binary Alloy Tests

To evaluate the predictive capabilities of the ML models (for more details, see **Supplementary 1**) for predicting the critical cooling rates in binary alloy systems, we employ a rigorous leave-one-system-out approach. The model is trained on all, except one binary system and then tested on the alloys in the excluded system. We then repeat this for every binary system. This method provides a rigorous assessment of the model's generalization and predictability capabilities on unseen data. Mean absolute percentage error (MAPE) is used as one of the metrics to evaluate the accuracy of the ML model, which represents the average of the absolute differences between the predicted and actual values, expressed as a percentage. The smaller the MAPE, the more accurate the model.

Table 1 summarizes all quantitative and statistical predictive performance of the various ML models when using different features, different datasets, and different strategies for separating training and testing data. All predictions for the binary systems are shown in Figure 3, for the ternary BMGs systems in Figure 5 (a) and for the sputtered ternary systems in Figure 5 (b).

When training and testing sets are not carefully separated at the alloy system level [14], a very small MAPE can be obtained, incorrectly suggesting high predictability. For example, randomly splitting all alloys into 90% training and 10% testing can yield a MAPE of ~1%, as alloys from the same system may appear in both sets. In this case, the model does not truly learn or predict, but instead performs trivial interpolation, and is therefore not useful for genuine predictions [14].

To avoid such issues, all model development in this work is carried out by separating data at the system level. Specifically, a leave-one-

Table 1
Summary of average predictions of neural network (NN), random forest (RF), and large language models. Feature sets are physically informed (PI), elemental properties (EP), composition (Comp), random (Random), and features generated by ChatGPT and Gemini (Supplementary 1.2.4). Data sets are sputtered binary, sputtered ternary, and BMGs ternary alloys. The models are trained on the sputtered binary data and validated by leaving out one binary system at a time; L2O removes all systems containing either test element from training; min reports the MAPE at the minimum R_c of each binary system.

Models \ Features	PI	EP	Comp	Random	Benchmark
RF by binary alloys	1.61% ± 0.01%	0.39% ± 0.01%	0.55% ± 0.01%	30.48% ± 0.01%	27.71%
RF by binary systems	17.62% ± 0.04%	24.53% ± 0.24%	27.40% ± 0.29%	30.83% ± 0.01%	27.71%
NN by binary systems	18.43% ± 0.3%	23.51% ± 0.43%	30.92%	-	27.71%
RF by binary systems (min)	33.48% ± 0.04%	48.57% ± 0.40%	56.55% ± 0.84%	59.13% ± 0.01%	27.71%
RF by binary systems (L2O)	20.26% ± 0.02%	28.93%	33.42%	30.76%	27.71%
RF by sputtered ternary systems	36.38%	-	-	-	44.66%
RF by BMGs ternary system	88.92%	-	-	-	265.41%
ChatGPT by binary systems	22.60%	-	-	-	27.71%
Gemini by binary systems	25.27%	-	-	-	27.71%

system-out scheme is adopted, in which all compositions belonging to one alloy system are left out for testing, while the remaining systems are used for training. Within the training systems, 10-fold cross-validation is performed to determine the optimal hyperparameters of the Random Forest model. The final model is then trained on all training systems and evaluated on the left-out system. This procedure is repeated for each system to obtain the reported model performance.

The highest statistically meaningful predictions with a MAPE ~18 % are achieved when random forest or neural networks in conjunction with Physically Informed Features are used to predict R_c. To evaluate whether such a MAPE indicates a successful model, we introduce a simple linear interpolation benchmark model to quantitatively compare the predictions of our ML models. In this benchmark model, we assume if two elements of a binary system have the same crystal structure, the R_c of all alloys within the alloy system will be 10^{14} K/s. If two elements of a binary system have different crystal structures, R_c as a function of composition in such an alloy system is a line whose middle point $A_{50}B_{50}$ is at 10^8 K/s and is connected to values for $R_c = 10^{14}$ K/s for pure A and pure B. This very simple benchmark model, using only minimal physical insight yields a MAPE of ~28%. Therefore, any developed ML model that learned the problem of glass-forming ability should yield a distinctly lower MAPE than the benchmark model.

To further separate training and test data, all alloys containing A **or** B (rather than only alloys containing A and B) were deliberately excluded from the training dataset. Subsequently, the trained model was tested on the A-B binary system. The test yields a MAPE of 20% (shown in Table 1: RF by binary systems (L2O)), higher but still similar to the 18% error level from the leave-one-system-out test (containing A and B), and still significantly smaller than the MAPE of ~28% for the benchmark model, indicating the model's robust extrapolation capabilities to new elements. This outcome is particularly significant as it demonstrates the model's potential in predicting the glass-forming ability of entirely new alloy systems.

One of the most challenging aspects of developing effective ML algorithms for complex materials science problems is selecting features that best represent the target label, here R_c. In this work, we use Physically Informed (PI), Elemental Properties (EP), Composition (Comp) and Random (Random) features, which we compare to the benchmark (results shown in Table 1). To further explore automated feature generation, we also employed large language models, such as ChatGPT and Gemini. The PI features achieve the best prediction, with a MAPE of 17.62%. The PI features demonstrate superior performance compared to features generated by large language models such as ChatGPT (22.60%) and Gemini (25.27%), as well as EP features (24.53%). In contrast, composition features (27.40%) and random features (30.83%) lead to substantially higher errors. These results highlight that incorporating physically meaningful descriptors (features) is important to accurately model the alloy behavior. Current large language models achieve slightly better prediction than EP features that do not contain mixing information but only alloy constituent information. However, they fall short when compared to PI features, which incorporate insights into the mixing of the constituent elements into alloys.

3.2. *ML Performance in Leave-One-System-Out Unknown Binary Alloy Tests*

After developing the ML algorithms, we use them to predict the critical cooling rates for alloy systems that are not included in the training data. We choose 16 practical elements and generate, out of all combinations, 94 binary alloy systems that have not been used for training or testing to explore the predictive capability of the model in previously unexplored compositional spaces. The random forest model trained using the PI feature and validated as the most accurate model through the leave-one-system-out approach described above is applied to these systems. The predictive reliability of the model has been established through leave-one-system-out cross-validation. The trained model is then applied to predict new alloy systems that extend beyond the experimental data considered here (Figure 2) and have mostly not yet been experimentally studied for glass formation, making direct quantitative validation currently unavailable. Instead, the predictions are interpreted based on model consistency and underlying physical trends (for more details, see **Supplementary 2.2**). Among these systems, our model predicts that BMg, BY, BMo, BPt, BNb, BW, BTa, PY, and CoNb alloy systems contain alloys with critical cooling rates below 10^5 K/s, suggesting that they may be practical glass-forming alloys. In particular, systems involving boron combined with transition or refractory metals (e.g., BNb, BTa, BW, BMo) consistently show low predicted R_c, suggesting high glass-forming ability, which is qualitatively consistent with empirical criteria such as large atomic size mismatch and negative Miedema-based mixing enthalpy, which are present in these systems. CoNb, here predicted with a critical cooling rates below 10^6 K/s is similar to the known, almost bulk metallic glass former NiNb [76–78], and Co and Ni are similar in size, have similar Miedema-based mixing enthalpy with Nb, and similar phase diagrams with Nb [76,77], and in higher-order glass formers, Co has been used as a replacement for Ni to improve GFA [79]. Phosphorus (P), here in several alloys with predicted critical cooling rates of approximately 10^8 K/s is widely used as an alloying element in metallic glass systems, particularly in transition metal-based alloys, due to its strong negative Miedema-based mixing enthalpy and its ability to promote glass formation [78,80,81], due to its

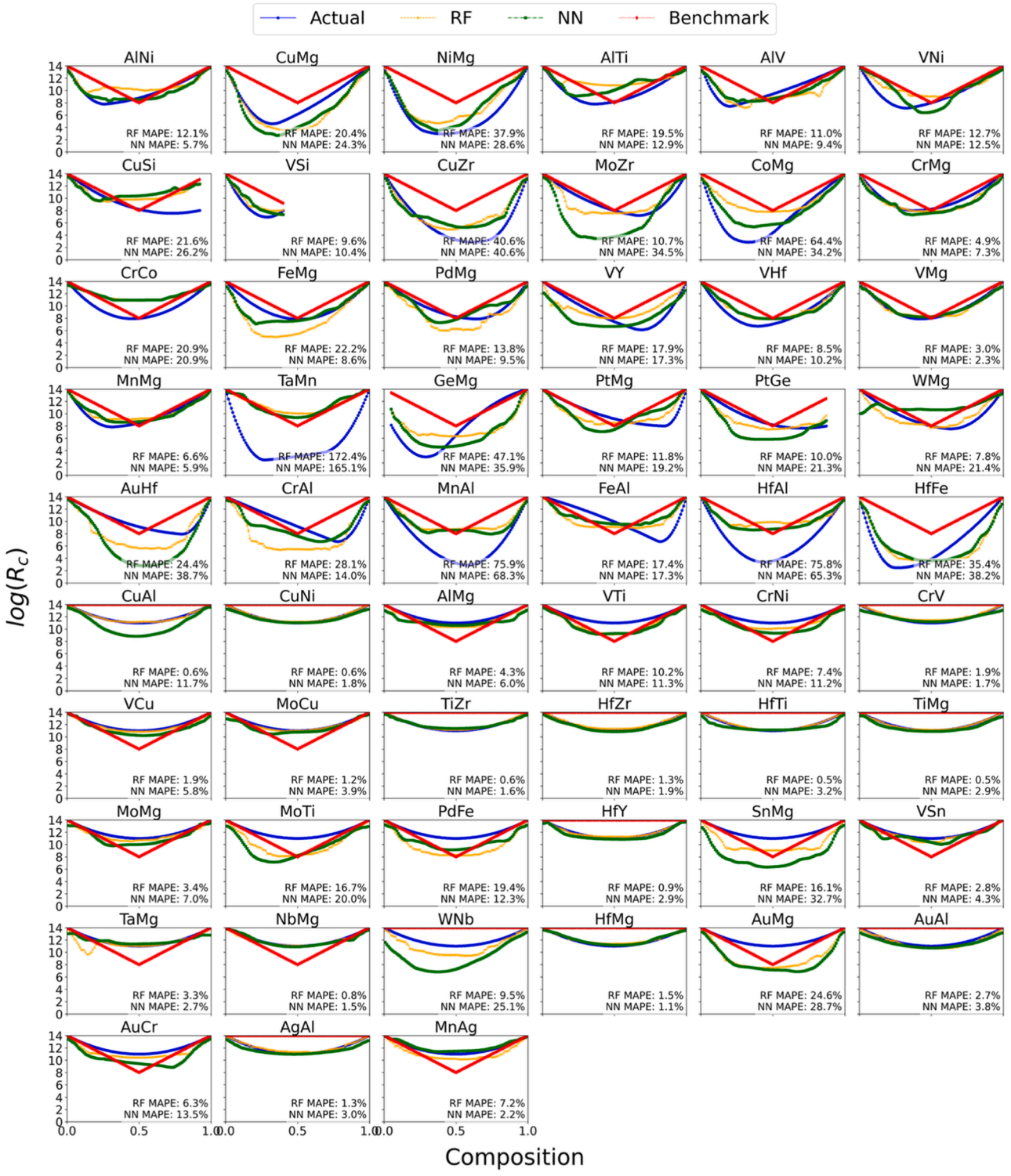


Figure 3. Evaluation of the ML model's performance using a leave-one-system-out validation method for selected sputtered binary alloy systems with PI feature set. Each subplot represents the comparison between actual and predicted critical cooling rates for a unique alloy system that has not been included in the training set. The blue lines denote the actual critical cooling rates, which are determined as explained above. The orange lines indicate the predicted rates from Random Forest (2nd row in Table 1); the green lines indicate the predicted rates from Neural Networks. The benchmark values are represented as red lines (for more details, see **Supplementary 2.1**).

size and large negative Miedema-based mixing enthalpy with transition metal elements.

In contrast, for the majority of the considered alloy systems, consistently high R_c values across the entire composition range are predicted by the algorithm, indicating poor glass-forming ability and suggesting that they are unlikely to form metallic glasses under practical cooling conditions. Overall, the model captures general distinctions between promising and unfavorable systems and may serve as a screening tool to identify candidate alloys for experimental validation.

To further evaluate the model and how it is able to predict general

glass-forming ability trends we compare each unknown alloy with alloys in the training set that are most similar in their features. An effective ML model can be expected to have the following characteristic: *if two alloys have similar features, one can conclude that they have similar R_c*. To explore whether such a characteristic is present for the developed ML model we compute, for each unknown alloy, its feature distance to the training data and organize the training systems from most similar to least similar (Figure 4), (for more calculation details, see **Supplementary 2.2**). For each alloy in the training set, R_c is also stated and color-coded. Such analysis and depiction reveal a strong correlation of the characteristic: *if two alloys have similar features one can conclude that they have similar R_c*. Specifically, unknown systems with nearest neighbors in feature space exhibiting low critical cooling rates consistently yield low predicted R_c values, indicating a strong local smoothness in the mapping between features and R_c. Conversely, when the nearest neighbors (in feature space) possess high R_c values, the predictions shift accordingly. This behavior confirms that the machine learning model effectively interpolates within well-represented regions of the feature space [31].

3.3. ML Performance in Leave-One-System-Out Ternary Alloy Tests

We also explored whether one could develop an ML model on binary alloys and use it to predict R_c in ternary alloys. Such a capability of an ML model would be extremely exciting as it would suggest that training on a small, and more importantly, less complex and restricted set of data could be used to predict glass formation in the exponentially larger higher-order systems [82]. Further, it would provide insights into the mechanism controlling glass formation. To explore this strategy, we use 385 ternary alloys that contain BMGs [3,18,83] and further use 9 ternary systems that have been sputtered and have been identified as amorphous vs crystalline. The ML model we use has been trained on the sputtered binary data and uses Physically Informed features (for more details, see **Supplementary 3.1**).

The overall MAPE is ~89% (for more details, see **Supplementary 3.1.1**) relative to the 265.41% ternary BMGs benchmark (for more details about the ternary benchmark, see **Supplementary 3.1.2(a)**) which is not particularly useful for quantitative comparison. For example, for a predicted $R_c = 10^7$ K/s the error would span approximately from $10^{0.77}$ to $10^{13.2}$ K/s. Surprisingly for some specific alloys can be predicted well (top row of Figure 5 (a)), even when their corresponding binary subsystems are not included in the training data. Generally, however, the prediction is very poor (bottom row of Figure 5 (a)). This may originate from a different motivation for glass formation at cooling rates that allow BMG formation, $R_c \leq 10^3$ K/s than during fast cooling [69]. To decouple the effect of training on binary systems and predicting ternary systems and the prediction of BMG from sputtered data, we also made predictions for ternary alloy systems for which ternary sputtering data on glass formation are available (Figure 5 (b)). For this task, we determine a MAPE of 36% relative to the 44.66% sputtered ternary benchmark (for more details about ternary benchmark, see **Supplementary 3.1.2(b)**). Such MAPE is lower than for the ternary BMGs but still not useful. For example, for a predicted $R_c = 10^7$ K/s the error would span approximately from $10^{4.48}$ to $10^{9.5}$ K/s. We argue that the poor predictability of ML algorithms trained on binary data and predicting into ternary system originates from the additional complexity and mixing terms present in ternary alloys that are not represented in the binary training data.

4. Discussion

We will now discuss the origins of the improvements of the binary ML models introduced here over previously reported ML models [2–4,6,12,38,84,85]. The improvement can be seen in the quality of the predictions. Previous models to predict metallic glasses mainly place predictions composition wise near existing BMGs that have been part of the training set rather than identifying unexplored and compositionally distinct alloy systems (see detailed discussion in **Supplementary 4**). Although previous ML studies of glass-forming ability report high classification accuracy, their datasets are heavily imbalanced toward glass-forming compositions. Thus, accuracy overstates performance while obscuring low precision and recall on the rare class of high glass formers. To avoid this problem, our work uses a regression formulation that directly predicts log (R_c) rather than classifying glass formation. Our method provides a continuous and imbalance-robust measure of glass-forming ability. The ML models introduced here also demonstrate predictive capability in unknown binary systems with quantitative validation (see **Supplementary 3.1.3).** We argue that the improvement of the ML models developed here originates from:

***Regression vs classification (Binary vs. Continuous Labeling)*:** Previous machine learning studies on glass-forming ability (GFA) mainly rely on classification frameworks. Typically, a binary labeling is chosen where an arbitrary cutoff for the cooling rate is selected, and alloys are classified by verifying or crystallizing under this cooling rate. Such models predict with high accuracy, which is quantified in the 90/10 cross-validation [3,4,17,83]. Using our data with binary labeling, and the same Physically Informed (PI) features, and our random forest model we achieve an accuracy of ~85%, comparable to previously reported models [2–4,6,12,38,84,85]. However, we argue that the usefulness of a classification is limited for predicting metallic glass-forming ability (GFA). GFA is fundamentally governed by the critical cooling rate R_c [28,56,86], and binary labels cannot capture its quantitative variation spanning ~14 orders of magnitude. We are addressing this limitation here by experimentally determining the critical cooling rate for some alloys, which allows us to interpolate in between these experimental data to estimate the GFA of every considered alloy by R_c (see 2.2 and Fig. 2). This reduces the quantifiable accuracy (MAPE) of the model because it compares with and predicts data varying by ~14 orders of magnitude. However, the usefulness of the prediction is much higher than in the classification, where the only prediction is whether an alloy is above or below an arbitrarily chosen R_c, whereas the here presented regression model directly predicts R_c.

***Data representation bias*:** Previous ML models to predict BMGs rely on training data that have been collected from the published literature [2–4,6,12,38,84,85]. Due to the tendency to publish positive data, such datasets are highly biased towards BMG formation, ~one BMG former per two alloys. This is in sharp contrast to the estimated likelihood that an alloy forms a BMG of ~one BMG former per one million alloys [23]. To address this data representation bias that previous ML models have been trained on [2–4,6,12,38,84,85], we construct a random and unbiased dataset from a representative fraction (~20%) of all binary alloys. Specifically, we use 57 random binary alloys and determine for 66 alloys per alloy system their structure and R_c (Fig. 1 and Fig. 2).

***Feature Representation and Bridging Elemental Properties to Alloy Features*:** Mixing effects in alloys can be complex, result in non-obvious behavior, and are complicated to describe quantitatively. For binary alloys, such mixing is significantly less complicated than for higher-order alloys; the mixing of two elements produces only one mixing interaction ε_{AB}, whereas for a ternary system, it produces three, ε_{AB}, ε_{AC}, ε_{CB} (for quaternary six). It is important to mention that not only does the number of the mixing interactions increase rapidly with the number of alloy components, but it is even more challenging to determine which of the interactions (ε_{AA}, ε_{BB}, ε_{AB}, for binary alloys and ε_{AA}, ε_{BB}, ε_{CC}, ε_{AB}, ε_{AC}, ε_{CB}, for ternary alloys) and their relative magnitudes define the overall mixing behavior and the corresponding property [31,37,82,87–90]. For binary alloys, mixing models have been developed, including models to describe the enthalpy of an alloy, the effect of atomic size difference on packing and structure, and the effect of element structure on the alloy structure. We use such quantifiable descriptions as features (see 2.3) to describe the alloy and its mixing with respect to glass-forming ability. Due to the absence of such models to describe GFA in ternary alloys for most characteristics (see 2.3 for heat of mixing, and atomic structure mismatch), applying such models for binary alloys results in better

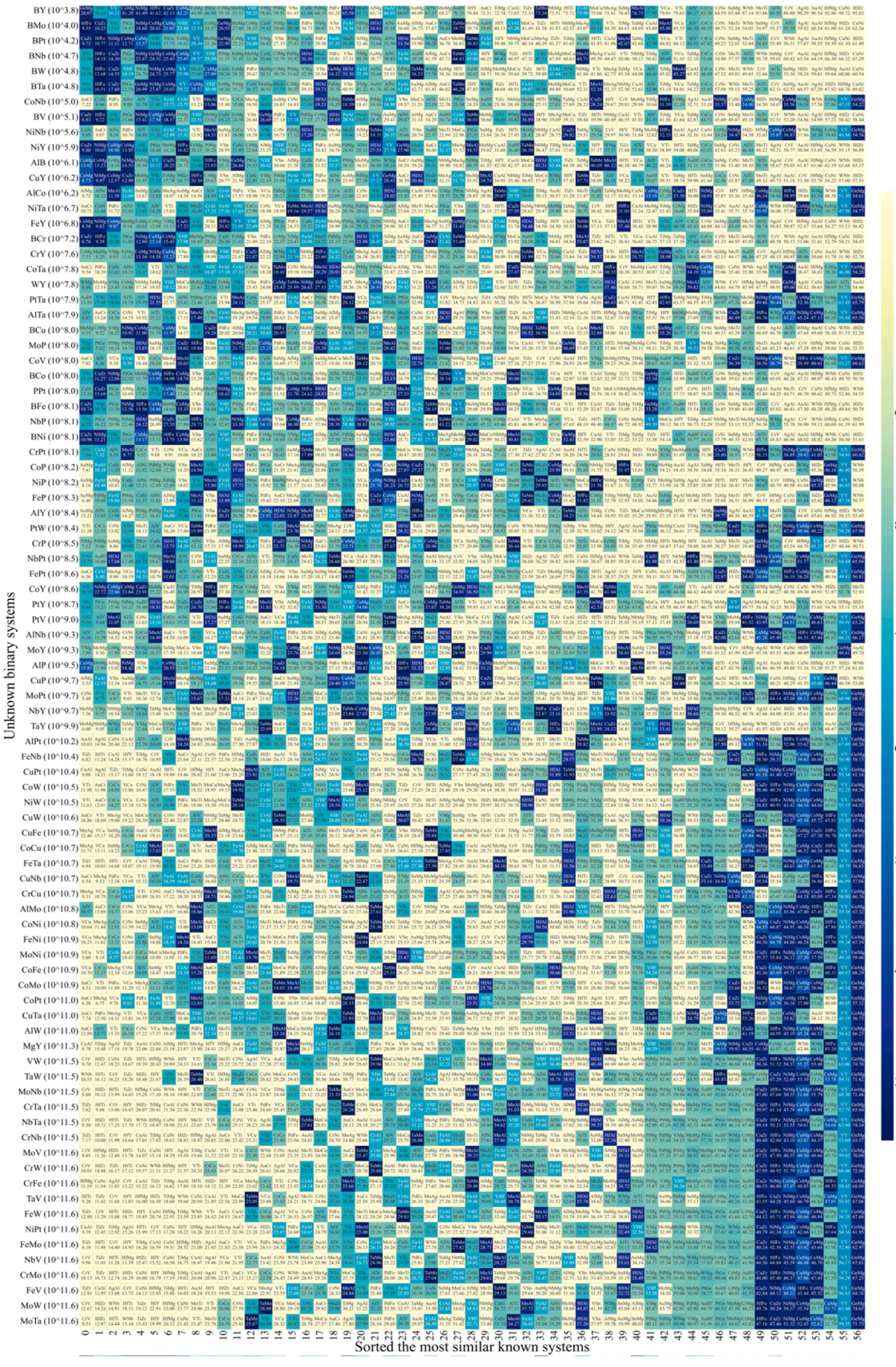


Figure 4. The Feature-distance-sorted heatmap shows the relationship between the feature similarity and the prediction of R_c of unknown binary systems. Unknown binary alloy systems are ordered by their predicted minimum R_c, while known systems used for the training are ranked by increasing feature distance (from left to right). The color of each cell corresponds to the minimum R_c of the known system, and annotations provide system identity and pairwise feature distance (for more details, see **Supplementary 2.2**).

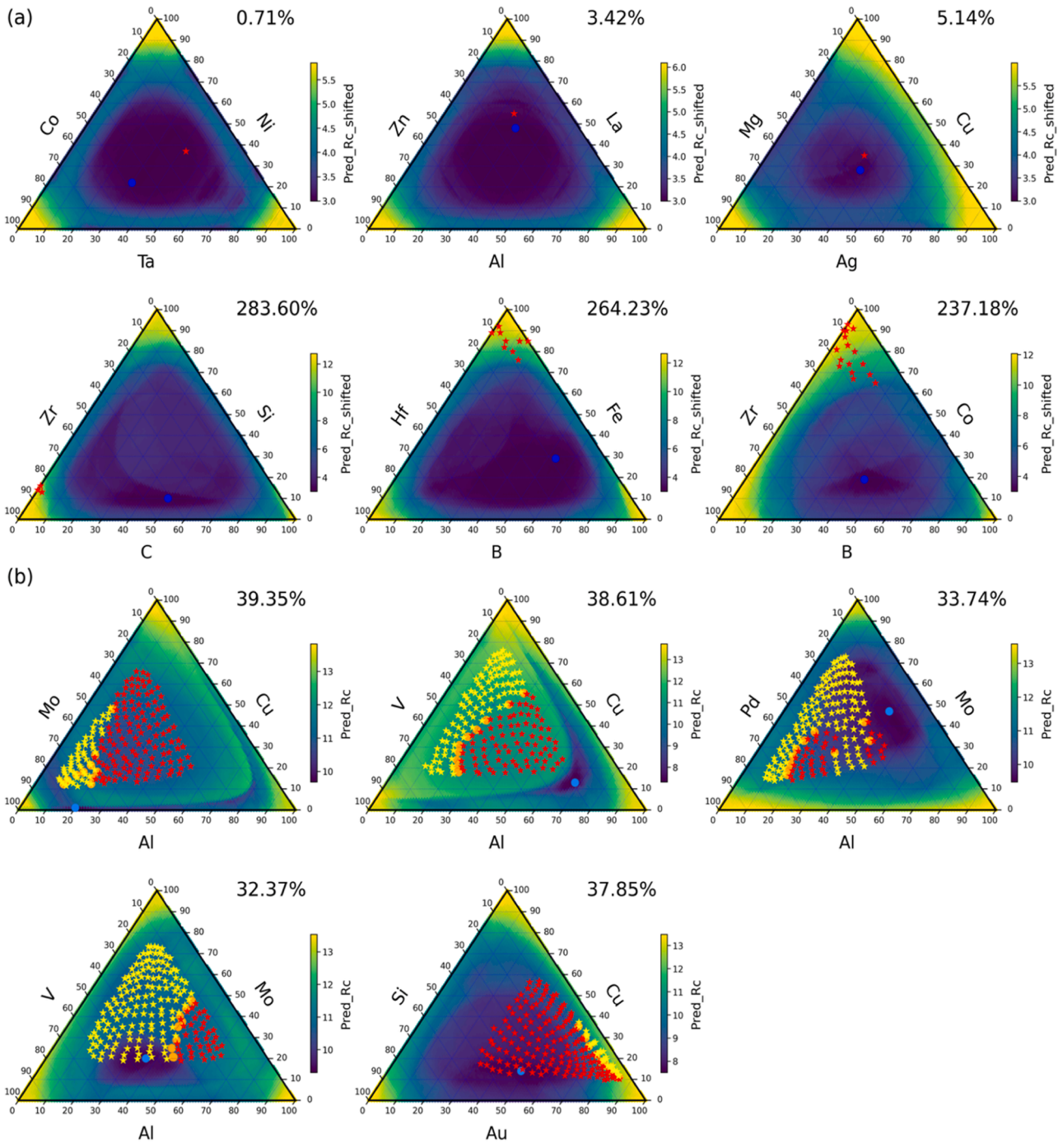


Figure 5. Examples of the most accurate and least accurate predictions of glass formation in ternary alloys using the Random Forest model and trained on the sputtered binary alloy systems with PI feature. (a) ternary BMGs systems: the upper three figures show the ternary systems for which we obtain the most accurate predictions and the lower three figures the least accurate predictions. The red stars indicate known BMG alloys, and the blue dots are the composition predicted by the model with the lowest R_c in each ternary alloy system. Pred_Rc_shifted means the shifted predictions of log (R_c) (for more details, see **Supplementary 3.1.1**). (b) Sputtered ternary systems: the red stars are the measured amorphous alloys. The yellow stars are the measured crystalline alloys. The orange dots are the calculated boundary points between crystalline and amorphous. Pred_Rc means the predictions of log (R_c).

feature representation of the alloys. Our finding that the ML model developed for binary alloys is highly inefficient when used to predict ternary alloy also reflects the missing ternary interactions and the understanding of how they affect GFA in ternary alloys.

***Subgrouping, Specificity and Accuracy of General Models*:** It is generally understood that a low R_c (high GFA) requires a dense packing of the alloy in its liquid state [36,88,91–96]. However, such dense packing is achieved by different strategies in binary vs ternary or higher-order systems [37,89,97]. Here, ML models are developed for binary alloys where motifs reflected in the features of glass formation in binary systems have been considered. This makes these models perform significantly better when predicting unknown binary systems than when predicting ternary systems, even for some cases where binary data have been used in the training of the ML model.

Overall, the ML model developed here to predict GFA, quantified by the critical cooling rate constitutes an improvement over the previous

ML models through addressing the above discussed issues in previous models. However, as we discussed previously [14], we argue that precise predictions for complex properties like the critical cooling rate using ML models will be always prohibited by the discreteness and small number of the atomic elements. At the same time, they are limited to binary alloys. Using the ML model trained on binary alloys to predict GFA in ternary alloys fails. This limitation arises from the increased complexity of interactions in ternary alloys, which are not present in the binary systems.

5. Conclusion

When limiting the applicable range and addressing previously identified issues, ML models can be developed that show some characteristics of true predictions of glass-forming ability in binary alloys. The specific issues that have been addressed here are: a.) the use of representative data, b.) subgrouping, c.) effective feature representation, and d.) continuous labeling (regression vs classification).

An overall mean absolute percentage error, MAPE of ~18% can be achieved for the best ML models developed here, significantly outperforming benchmark models (~28%) that we developed for comparison. True learning is indicated by the finding that alloys with similar features (small feature distance) exhibit similar critical cooling rates.

Using the ML models developed here, which are trained on binary alloys, to predict ternary alloys is ineffective, and we provide arguments that the complexity of the mixing in ternary alloys, which is not represented, and therefore learned in the binary systems is the main reason for it.

Overall, the ML models developed here show some predictability, which is reflected in their learning of the underlying feature relationships. However, such predictions are far from being precise. We argue that precise predictions of the critical cooling rate are ultimately limited by the most fundamental characteristic of atomic elements, their discreteness in properties and small number of different elements.

Declaration of generative AI and AI-assisted technologies in the manuscript preparation process

During the preparation of this work, the author(s) used ChatGPT and Gemini to quantify the ability of LLMs to identify features for machine learning approaches. The author(s) reviewed and edited the output as needed and take full responsibility for the content of the published article.

CRediT authorship contribution statement

Yifei He: Writing – review & editing, Writing – original draft, Visualization, Validation, Software, Methodology, Investigation, Formal analysis, Data curation. **Guannan Liu:** Writing – original draft, Software, Funding acquisition, Data curation, Conceptualization. **Salena Huang:** Writing – review & editing, Resources, Investigation. **Sebastian Kube:** Methodology. **Sungwoo Sohn:** Writing – review & editing, Formal analysis. **Xiaorui Xiong:** Software. **Mark D. Shattuck:** Writing – review & editing, Formal analysis. **Corey S. O'Hern:** Writing – review & editing, Formal analysis. **Anna Gilbert:** Writing – review & editing, Formal analysis. **Jan Schroers:** Writing – review & editing, Writing – original draft, Validation, Supervision, Project administration, Methodology, Funding acquisition, Conceptualization.

Declaration of competing interest

The authors declare that they have no known competing financial interests or personal relationships that could have appeared to influence the work reported in this paper.

Acknowledgements

This work was financially supported by the National Science Foundation through NSF-DMR (grant no. 2104316), NSF DGE2244310 (C.S. O), and the feature generation through CMMI 2311311.

Supplementary materials

Supplementary material associated with this article can be found, in the online version, at doi:10.1016/j.actamat.2026.122807.

References

[1] Y.T. Sun, H.Y. Bai, M.Z. Li, W.H. Wang, Machine Learning Approach for Prediction and Understanding of Glass-Forming Ability, J Phys Chem Lett 8 (14) (2017) 3434–3439.
[2] C. Liu, X. Wang, W. Cai, Y. He, H. Su, Machine Learning Aided Prediction of Glass-Forming Ability of Metallic Glass, Processes 11 (9) (2023) 2806.
[3] L. Ward, S.C. O'Keeffe, J. Stevick, G.R. Jelbert, M. Aykol, C. Wolverton, A machine learning approach for engineering bulk metallic glass alloys, Acta Mater 159 (2018) 102–111.
[4] G.N. Liu, S. Sohn, S.A. Kube, A. Raj, A. Mertz, A. Nawano, A. Gilbert, M. D. Shattuck, C.S. O'Hern, J. Schroers, Machine learning versus human learning in predicting glass-forming ability of metallic glasses (vol 243, 118497, 2023), Acta Mater 255 (2023).
[5] A. Ghorbani, A. Askari, M. Malekan, M. Nili-Ahmadabadi, Thermodynamically-guided machine learning modelling for predicting the glass-forming ability of bulk metallic glasses, Sci Rep-Uk 12 (1) (2022) 11754.
[6] O.A. Graeve, M.S. García-Vázquez, A.A. Ramírez-Acosta, Z. Cadieux, Latest Advances in Manufacturing and Machine Learning of Bulk Metallic Glasses, Adv Eng Mater 25 (9) (2023) 2201493.
[7] R.M. Forrest, A.L. Greer, Evolutionary design of machine-learning-predicted bulk metallic glasses, Digital Discovery 2 (1) (2023) 202–218.
[8] X. Liu, J. Zhang, Z. Pei, Machine learning for high-entropy alloys: Progress, challenges and opportunities, Prog Mater Sci 131 (2023) 101018.
[9] K. Kaufmann, K.S. Vecchio, Searching for high entropy alloys: A machine learning approach, Acta Mater 198 (2020) 178–222.
[10] Y.M. Zhao, J.Y. Zhang, P.K. Liaw, T. Yang, Machine Learning-Based Computational Design Methods for High-Entropy Alloys, High Entropy Alloys & Materials 3 (1) (2025) 41–100.
[11] P. Liu, H. Huang, S. Antonov, C. Wen, D. Xue, H. Chen, L. Li, Q. Feng, T. Omori, Y. Su, Machine learning assisted design of γ′-strengthened Co-base superalloys with multi-performance optimization, Npj Comput Mater 6 (1) (2020) 62.
[12] G.L.W. Hart, T. Mueller, C. Toher, S. Curtarolo, Machine learning for alloys, Nat Rev Mater 6 (8) (2021) 730–755.
[13] Y. Gu, C.D. Stiles, J.A. El-Awady, A statistical perspective for predicting the strength of metals: Revisiting the Hall–Petch relationship using machine learning, Acta Mater 266 (2024) 119631.
[14] Y. He, I. Katsman, G. Liu, S. Sohn, M.D. Shattuck, C.S. O'Hern, A. Gilbert, J. Schroers, Can machine learning predict the liquidus temperature of binary alloys? Acta Mater 312 (2026) 122220.
[15] G. Deffrennes, K. Terayama, T. Abe, E. Ogamino, R. Tamura, A framework to predict binary liquidus by combining machine learning and CALPHAD assessments, Mater Design 232 (2023) 112111.
[16] G. Liu, S. Sohn, S.A. Kube, A. Raj, A. Mertz, A. Nawano, A. Gilbert, M.D. Shattuck, C.S. O'Hern, J. Schroers, Machine learning versus human learning in predicting glass-forming ability of metallic glasses, Acta Materialia 243 (2023) 118497.
[17] X. Liu, X. Li, Q. He, D. Liang, Z. Zhou, J. Ma, Y. Yang, J. Shen, Machine learning-based glass formation prediction in multicomponent alloys, Acta Mater 201 (2020) 182–190.
[18] L. Ward, A. Agrawal, A. Choudhary, C. Wolverton, A general-purpose machine learning framework for predicting properties of inorganic materials, Npj Comput Mater 2 (1) (2016) 16028.
[19] V. Stanev, C. Oses, A.G. Kusne, E. Rodriguez, J. Paglione, S. Curtarolo, I. Takeuchi, Machine learning modeling of superconducting critical temperature, Npj Comput Mater 4 (2018).
[20] P. Bordeenithikasem, J.B. Liu, S.A. Kube, Y.L. Li, T.X. Ma, B.E. Scanley, C. C. Broadbridge, J.J. Vlassak, J.P. Singer, J. Schroers, Determination of critical cooling rates in metallic glass forming alloy libraries through laser spike annealing (vol 7, 7155, 2017), Sci Rep-Uk 8 (2018).
[21] S. Huang, S.A. Kube, N.S. Johnson, S. Sohn, A. Mehta, J. Schroers, Glass formation during combinatorial sputtering in binary alloys, Acta Mater 296 (2025) 121240.
[22] P. Domingos, A few useful things to know about machine learning, Communications of the ACM 55 (10) (2012) 78–87.
[23] Y.L. Li, S.F. Zhao, Y.H. Liu, P. Gong, J. Schroers, How Many Bulk Metallic Glasses Are There? Acs Comb Sci 19 (11) (2017) 687–693.
[24] H. He, E.A. Garcia, Learning from imbalanced data, IEEE Transactions on knowledge and data engineering 21 (9) (2009) 1263–1284.
[25] X. Gong, J. Bi, X. Liu, R. Li, R. Xiao, T. Zhang, H. Li, Efficient learning strategy for predicting glass forming ability in imbalanced datasets of bulk metallic glasses, Phys Rev Mater 8 (5) (2024) 055602.

[26] G.M. Weiss, Mining with rarity: a unifying framework, ACM Sigkdd Explorations Newsletter 6 (1) (2004) 7–19.
[27] N.V. Chawla, K.W. Bowyer, L.O. Hall, W.P. Kegelmeyer, SMOTE: synthetic minority over-sampling technique, Journal of artificial intelligence research 16 (2002) 321–357.
[28] J. Schroers, Bulk Metallic Glasses, Phys Today 66 (2) (2013) 32.
[29] A. Inoue, Stabilization of metallic supercooled liquid and bulk amorphous alloys, Acta Mater 48 (1) (2000) 279–306.
[30] D.B. Miracle, O.N. Senkov, A critical review of high entropy alloys and related concepts, Acta Mater 122 (2017) 448–511.
[31] S.A. Kube, S. Sohn, D. Uhl, A. Datye, A. Mehta, J. Schroers, Phase selection motifs in High Entropy Alloys revealed through combinatorial methods: Large atomic size difference favors BCC over FCC, Acta Mater 166 (2019) 677–686.
[32] T. Chookajorn, H.A. Murdoch, C.A. Schuh, Design of stable nanocrystalline alloys, Science 337 (6097) (2012) 951–954.
[33] B.E. Scanley, W.T. Xing, S.A. Kube, A.R. Kalidindi, D. Amram, J. Schroers, C. A. Schuh, Stability of ternary nanocrystalline alloys in the Pt-Pd-Au system, Materialia 8 (2019) 100449.
[34] S.A. Kube, W.Y. Xing, A. Kalidindi, S. Sohn, A. Datye, D. Amram, C.A. Schuh, J. Schroers, Combinatorial study of thermal stability in ternary nanocrystalline alloys, Acta Mater 188 (2020) 40–48.
[35] B.J. Wieder, B. Bradlyn, J. Cano, Z. Wang, M.G. Vergniory, L. Elcoro, A. A. Soluyanov, C. Felser, T. Neupert, N. Regnault, Topological materials discovery from crystal symmetry, Nat Rev Mater 7 (3) (2022) 196–216.
[36] T. Egami, Y. Waseda, Atomic Size Effect on the Formability of Metallic Glasses, J Non-Cryst Solids 64 (1-2) (1984) 113–134.
[37] A. Takeuchi, A. Inoue, Classification of bulk metallic glasses by atomic size difference, heat of mixing and period of constituent elements and its application to characterization of the main alloying element, Mater Trans 46 (12) (2005) 2817–2829.
[38] G.N. Liu, S. Sohn, C.S. O'Hern, A.C. Gilbert, J. Schroers, Effective subgrouping enhances machine learning prediction in complex materials science phenomena: Inoue's subgrouping in discovering bulk metallic glasses, Acta Mater 265 (2024).
[39] A.L. Greer, M.B. Costa, O.S. Houghton, Metallic glasses, Mrs Bull 48 (10) (2023) 1054–1061.
[40] L. Behnke, E.T. Lund, A.K. Dutta, J.D. La Torre, S. Sohn, A.J. Horvath, S.-W. Lee, J. Schroers, Metallic glass wire-based springs, Mater Design (2026) 116626.
[41] M.X. Li, S.F. Zhao, Z. Lu, A. Hirata, P. Wen, H.Y. Bai, M.W. Chen, J. Schroers, Y. H. Liu, W.H. Wang, High-temperature bulk metallic glasses developed by combinatorial methods, Nature 569 (7754) (2019), 99–+.
[42] A. Inoue, B.L. Shen, H. Koshiba, H. Kato, A.R. Yavari, Cobalt-based bulk glassy alloy with ultrahigh strength and soft magnetic properties, Nat Mater 2 (10) (2003) 661–663.
[43] W. Chen, J. Ketkaew, Z. Liu, R.M.O. Mota, K. O'Brien, C.S. da Silva, J. Schroers, Does the fracture toughness of bulk metallic glasses scatter? Scripta Mater 107 (2015) 1–4.
[44] M.D. Demetriou, M.E. Launey, G. Garrett, J.P. Schramm, D.C. Hofmann, W. L. Johnson, R.O. Ritchie, A damage-tolerant glass, Nat Mater 10 (2) (2011) 123–128.
[45] J. Schroers, W.L. Johnson, Ductile bulk metallic glass, Phys Rev Lett 93 (25) (2004).
[46] L. Shao, J. Ketkaew, P. Gong, S.F. Zhao, S. Sohn, P. Bordeenithikasem, A. Datye, R. M.O. Mota, N.J. Liu, S.A. Kube, Y.H. Liu, W. Chen, K.F. Yao, S.J. Wu, J. Schroers, Effect of chemical composition on the fracture toughness of bulk metallic glasses, Materialia 12 (2020).
[47] S. Sohn, N. Liu, G.H. Yoo, A. Ochiai, J. Chen, C. Levitt, G. Liu, S.C. Schroers, E. T. Lund, E.S. Park, J. Schroers, A framework for plasticity in metallic glasses, Materialia 31 (2023) 101876.
[48] W.L. Johnson, K. Samwer, A universal criterion for plastic yielding of metallic glasses with a (T/T-g)(2/3) temperature dependence, Phys Rev Lett 95 (19) (2005).
[49] M.F. Ashby, A.L. Greer, Metallic glasses as structural materials, Scripta Mater 54 (3) (2006) 321–326.
[50] W. Chen, Z. Liu, J. Ketkaew, R.M.O. Mota, S.H. Kim, M. Power, W. Samela, J. Schroers, Flaw tolerance of metallic glasses, Acta Mater 107 (2016) 220–228.
[51] J. Schroers, Processing of Bulk Metallic Glass, Adv Mater 22 (14) (2010) 1566–1597.
[52] B. Zhang, D.Q. Zhao, M.X. Pan, W.H. Wang, A.L. Greer, Amorphous metallic plastic, Phys Rev Lett 94 (20) (2005).
[53] R.M.O. Mota, N.J. Liu, S.A. Kube, J. Chay, H.D. McClintock, J. Schroers, Overcoming geometric limitations in metallic glasses through stretch blow molding, Applied Materials Today 19 (2020).
[54] A.K. Dutta, J. Halperin, E.T. Lund, Z. Steinglass, L. Behnke, S. Sohn, J. Schroers, Continuous thermoplastic drawing of metallic glass wires and tubes, Applied Materials Today 50 (2026) 103286.
[55] Z. Liu, N. Liu, J. Schroers, Nanofabrication through molding, Prog Mater Sci 125 (2022) 100891.
[56] R. Busch, J. Schroers, W.H. Wang, Thermodynamics and kinetics of bulk metallic glass, Mrs Bull 32 (8) (2007) 620–623.
[57] T. Egami, C.W. Ryu, Why Is the Range of Timescale So Wide in Glass-Forming Liquid? Front Chem 8 (2020).
[58] N.J. Liu, S. Sohn, M.Y. Na, G.H. Park, A. Raj, G.N. Liu, S.A. Kube, F.S. Yuan, Y. H. Liu, H.J. Chang, J. Schroers, Size-dependent deformation behavior in nanosized amorphous metals suggesting transition from collective to individual atomic transport, Nat Commun 14 (1) (2023).
[59] M.E. Blodgett, T. Egami, Z. Nussinov, K.F. Kelton, Proposal for universality in the viscosity of metallic liquids, Sci Rep-Uk 5 (2015).
[60] T. Egami, Atomic level stresses, Prog Mater Sci 56 (6) (2011) 637–653.
[61] G.R. Garrett, M.D. Demetriou, M.E. Launey, W.L. Johnson, Origin of embrittlement in metallic glasses, P Natl Acad Sci USA 113 (37) (2016) 10257–10262.
[62] N.J. Liu, T.X. Ma, C.Q. Liao, G.N. Liu, R.M.O. Mota, J.B. Liu, S. Sohn, S. Kube, S. F. Zhao, J.P. Singer, J. Schroers, Combinatorial measurement of critical cooling rates in aluminum-base metallic glass forming alloys, Sci Rep-Uk 11 (1) (2021).
[63] K. Kelton, A.L. Greer, Nucleation in condensed matter: applications in materials and biology, Elsevier, 2010.
[64] D. Turnbull, Under what conditions can a glass be formed? Contemporary physics 10 (5) (1969) 473–488.
[65] N. Nishiyama, K. Takenaka, A. Inoue, Pd30Pt17.5Cu32.5P20 alloy with low critical cooling rate of 0.067 K/s, Appl Phys Lett 88 (12) (2006).
[66] T.A. Waniuk, J. Schroers, W.L. Johnson, Critical cooling rate and thermal stability of Zr-Ti-Cu-Ni-Be alloys, Appl Phys Lett 78 (9) (2001) 1213–1215.
[67] K. Hildal, N. Sekido, J.H. Perepezko, Critical cooling rate for Fe48Cr15Mo14Y2C15B6 bulk metallic glass formation, Intermetallics 14 (8-9) (2006) 898–902.
[68] L. Zhong, J.W. Wang, H.W. Sheng, Z. Zhang, S.X. Mao, Formation of monatomic metallic glasses through ultrafast liquid quenching, Nature 512 (7513) (2014), 177–+.
[69] Y.-C. Hu, J.T. Zhai, L.-H. Liu, W.W. Zhang, H.-Y. Bai, W.-H. Wang, H. Tanaka, Monatomic glass formation through competing order balance, Nat Commun 16 (1) (2025) 8183.
[70] Y.C. Hu, W.W. Jin, J. Schroers, M.D. Shattuck, C.S. O'Hern, Glass-forming ability of binary Lennard-Jones systems, Phys Rev Mater 6 (7) (2022).
[71] F. Spaepen, Structural Model for Solid-Liquid Interface in Monatomic Systems, Acta Metall Mater 23 (6) (1975) 729–743.
[72] Y. Li, Q. Guo, J.A. Kalb, C.V. Thompson, Matching Glass-Forming Ability with the Density of the Amorphous Phase, Science 322 (5909) (2008) 1816–1819.
[73] W.L. Johnson, J.H. Na, M.D. Demetriou, Quantifying the origin of metallic glass formation, Nat Commun 7 (2016).
[74] D.B. Miracle, D.V. Louzguine-Luzgin, L.V. Louzguina-Luzgina, A. Inoue, An assessment of binary metallic glasses: correlations between structure, glass forming ability and stability, International Materials Reviews 55 (4) (2010) 218–256.
[75] S.Y. Ding, Y.H. Liu, Y.L. Li, Z. Liu, S. Sohn, F.J. Walker, J. Schroers, Combinatorial development of bulk metallic glasses, Nat Mater 13 (5) (2014) 494–500.
[76] H. Choi-Yim, D.H. Xu, W.L. Johnson, Ni-based bulk metallic glass formation in the Ni-Nb-Sn and Ni-Nb-Sn-X (X = B,Fe,Cu) alloy systems, Appl Phys Lett 82 (7) (2003) 1030–1032.
[77] L. Xia, W.H. Li, S.S. Fang, B.C. Wei, Y.D. Dong, Binary Ni-Nb bulk metallic glasses, J Appl Phys 99 (2) (2006).
[78] L.M. Ruschel, O. Gross, B. Bochtler, B. Li, B. Adam, N. Neuber, M. Frey, S. Jakovlev, F. Yang, H.-R. Jiang, B. Gludovatz, J.J. Kruzic, R. Busch, Ni-Nb-P-based bulk glass-forming alloys: Superior material properties combined in one alloy family, Acta Mater 253 (2023) 118968.
[79] L. Zhang, M.J. Zhuo, J. Xu, Enhancing bulk metallic glass formation in Ni-Nb-Sn-based alloys via substitutional alloying with Co and Hf, J Mater Res 23 (3) (2008) 688–699.
[80] A. Drehman, A. Greer, D. Turnbull, Bulk formation of a metallic glass: Pd40Ni40P20, Appl Phys Lett 41 (8) (1982) 716–717.
[81] J. Schroers, W.L. Johnson, Highly processable bulk metallic glass-forming alloys in the Pt-Co-Ni-Cu-P system, Appl Phys Lett 84 (18) (2004) 3666–3668.
[82] S.A. Kube, J. Schroers, Metastability in high entropy alloys, Scripta Mater 186 (2020) 392–400.
[83] F. Ren, L. Ward, T. Williams, K.J. Laws, C. Wolverton, J. Hattrick-Simpers, A. Mehta, Accelerated discovery of metallic glasses through iteration of machine learning and high-throughput experiments, Sci Adv 4 (4) (2018).
[84] Y.T. Sun, H.Y. Bai, M.Z. Li, W.H. Wang, Machine Learning Approach for Prediction and Understanding of Glass-Forming Ability, The Journal of Physical Chemistry Letters 8 (14) (2017) 3434–3439.
[85] J. Xiong, S.-Q. Shi, T.-Y. Zhang, A machine-learning approach to predicting and understanding the properties of amorphous metallic alloys, Mater Design 187 (2020) 108378.
[86] D. Turnbull, Under What Conditions Can a Glass Be Formed, Contemporary Physics 10 (5) (1969), 473–&.
[87] A. Takeuchi, A. Inoue, Calculations of mixing enthalpy and mismatch entropy for ternary amorphous alloys, Mater T Jim 41 (11) (2000) 1372–1378.
[88] D.B. Miracle, A structural model for metallic glasses, Nat Mater 3 (10) (2004) 697–702.
[89] K. Zhang, B. Dice, Y.H. Liu, J. Schroers, M.D. Shattuck, C.S. O'Hern, On the origin of multi-component bulk metallic glasses: Atomic size mismatches and de-mixing, J Chem Phys 143 (5) (2015).
[90] M.A. Turchanin, P.G. Agraval, G.O. Vodopyanova, V.A. Korsun, Thermodynamic Properties of the Glass-Forming Ternary (Fe, Co, Ni, Cu)–Ti–Zr Liquid Alloys I. Mixing Enthalpies of Liquid Alloys, Powder Metallurgy and Metal Ceramics 62 (9) (2024) 621–631.
[91] B.C. Lu, J.H. Yao, J. Xu, Y. Li, A model of atom dense packing for metallic glasses with high-solute concentration, Appl Phys Lett 94 (24) (2009).
[92] H.W. Sheng, W.K. Luo, F.M. Alamgir, J.M. Bai, E. Ma, Atomic packing and short-to-medium-range order in metallic glasses, Nature 439 (7075) (2006) 419–425.
[93] A. Takeuchi, K. Yubuta, M. Ogata, A. Inoue, Molecular dynamics simulations of critically percolated, cluster-packed structure in Zr-Al-Ni bulk metallic glass, J Mater Sci 45 (18) (2010) 4898–4905.
[94] K.J. Laws, D.B. Miracle, M. Ferry, A predictive structural model for bulk metallic glasses, Nat Commun 6 (2015).

[95] K. Zhang, Y.H. Liu, J. Schroers, M.D. Shattuck, C.S. O'Hern, The glass-forming ability of model metal-metalloid alloys, J Chem Phys 142 (10) (2015).
[96] Y.Q. Cheng, E. Ma, Atomic-level structure and structure-property relationship in metallic glasses, Prog Mater Sci 56 (4) (2011) 379–473.
[97] D.V. Louzguine-Luzgin, D.B. Miracle, L. Louzguina-Luzgina, A. Inoue, Comparative analysis of glass-formation in binary, ternary, and multicomponent alloys, J Appl Phys 108 (10) (2010).